Journal of Colloid and Interface Science **229,** 261–273 (2000)
doi:10.1006/jcis.2000.7027, available online at http://www.idealibrary.com on IDEAL®

Fractal-like Aggregates: Relation between Morphology and Physical Properties

A. V. Filippov,[1] M. Zurita, and D. E. Rosner

Department of Chemical Engineering and Center for Combustion Studies, Yale University, New Haven, Connecticut 06520

Received March 13, 2000; accepted June 5, 2000

A number of modern technological applications require a detailed calculation of the physical properties of aggregated aerosol particles. For example, in probing soot aerosols by the method called laser-induced incandescence (LII), the soot clusters are suddenly heated by a short, powerful laser pulse and then cool down to the temperature of the carrier gas. LII sizing is based on rigorous calculation of the soot aggregate heat-up and cooling and involves prediction of laser light absorption and energy and mass transfer between aggregated particles and the ambient gas. This paper describes results of numerical simulations of the mass or energy transfer between the gas and fractal-like aggregates of N spherical particles in either the free-molecular or continuum regime, as well as the light scattering properties of random fractal-like aggregates, based on Rayleigh–Debye–Gans (RDG) theory. The aggregate geometries are generated numerically using specially developed algorithms allowing "tuning" of the fractal dimension and prefactor values. Our results are presented in the form of easily applicable scaling laws, with special attention paid to relations between the aggregate gyration radius and the effective radius describing various transport processes between the aggregates and the carrier gas.

Key Words: **fractal dimension; aggregate numerical generation; RDG theory; energy and mass transfer; scaling laws; quasi-Monte Carlo method; multipole expansion.**

1. INTRODUCTION

The transfer of mass, energy, and momentum between small, suspended particles and a gaseous environment, and the transport properties of the particles themselves, are subjects of considerable technological importance. Various ultrafine powders, such as carbon black, titania, and silica, are routinely produced by vapor-condensation combustion synthesis processes in industry. These particles are of technological importance because of their desirable optical, mechanical, catalytic, and electrical properties and remarkably high specific surface areas (associated with their nanometer-scale size). On the other hand, effective online and offline diagnostics of relevant industrial aerosol processes also require a detailed knowledge of various particle optical and physical parameters. For example, theoretical prediction of the particle-to-gas heat transfer under highly nonequilibrium conditions, diffusion transport, and heat conductivity cooling is necessary for correct interpretation of laser-induced incandescence (LII) signals (1). Accurate calculation of the basic physical properties of ultrafine particles is needed both for planning their technological applications and for optimizing the processes connected with their manufacturing.

The physics of highly dispersed aerosols consisting of single particles with a mean diameter <1 μm has been studied extensively during the past few decades (2). However, many aerosols actually consist of a number of small, nearly spherical particles (spherules) which join together to form tenuous "flocs" or aggregates, whose geometry is statistically described in terms of the concepts of fractal geometry (3). There are a wide variety of such particles, including metals, metal oxides, carbon, and SiO_2, usually having fractal dimensions between 1.7 and 1.9. Soot particles, too, are commonly in the form of aggregates of small spherules. The *fractal-like* aggregates, containing often some tens to some hundreds of spherules with a moderate ratio of the effective aggregate size to spherule size, require a very detailed analysis for prediction of their physical properties. There is still very little theoretical information about the transport and other properties of such aggregates, because the corresponding mathematical problems are substantially more difficult than for isolated spherules due to interspherule ("collective") shielding effects.

It is generally agreed that not only the aggregate *geometry* but also their basic *physical properties* fulfill specific scaling laws, which are typically postulated. In this paper, the corresponding scaling laws governing fractal-like aggregates are obtained by rigorous calculation of the main physical properties. In the free-molecular regime, the deterministic, low-discrepancy Halton sequences are used in the framework of the so-called quasi-Monte Carlo technique, which results in a substantial increase in computation efficiency when compared with conventional Monte Carlo calculations using the random number generation. Accurate continuum-regime calculations are performed using a multipole expansion technique (4). The fractal-like aggregate geometries are generated numerically, using two different

[1] To whom correspondence should be addressed. E-mail: andrey.filippov@yale.edu.

0021-9797/00 $35.00

"tunable" algorithms, described in detail in Section 2. Based on direct calculations, a variety of relevant ensemble-averaged dimensionless results, such as the structure factor for the light scattering, aggregate "accessible" area, distribution of the mass or energy transfer rates within the aggregates, and total transfer rates, are obtained as functions of the gyration radius and primary particle (spherule) number for different fractal dimensions. Until now, the shielding effect of the aggregated particles on their momentum and energy transfer rates has been estimated based on "plausible" *a priori* arguments (5), or the results of indirect measurements. The possibility of taking into account intermolecular collisions, to extend our results into the domain of intermediate Knudsen numbers will be investigated in future papers.

2. FRACTAL-LIKE AGGREGATES

Many aerosols are formed by the aggregation of small, nearly spherical particles into complex geometries which cannot be successfully approximated as dense or porous spheres or other simple shapes. Additional parameters are needed to characterize the morphology and basic physical properties of these aerosols, including mass, momentum, or energy transfer. The fractal-like nature of such aerosol aggregates, first noted probably by Forrest and Witten (6), is mathematically expressed through the following statistical scaling law:

$$N = k_f \left(\frac{R_g}{a} \right)^{D_f}, \qquad [1]$$

where a is the primary particle mean radius (assumed constant), k_f is the fractal prefactor, D_f is the fractal "dimension," N is the number of primary particles in the aggregate, and R_g is the radius of gyration. The usual geometrical radius of gyration is defined via the mean square of the distances between the spherule centers and the geometrical center of mass of the aggregate:

$$R_g^2 = \frac{1}{N} \sum_{i=1}^{N} (\mathbf{r}_i - \mathbf{r}_0)^2, \qquad [2]$$

$$\mathbf{r}_0 = \frac{1}{N} \sum_{i=1}^{N} \mathbf{r}_i, \qquad [3]$$

where $\mathbf{r}_i$ and $\mathbf{r}_0$ define respectively position of the ith spherule center and the center of the cluster composed of N identical spherules. Because the energy transfer and mass transfer, as well as chemical reactions between particles and the carrier gas, occur on the aggregate *surface*, a more consistent definition for the gyration radius of each aggregate would be the mean square distance between $\mathbf{r}_0$ and all points on the spherule *surfaces*, given by the equation

$$R_g^2 = \frac{1}{N} \sum_{i=1}^{N} (\mathbf{r}_i - \mathbf{r}_0)^2 + a^2. \qquad [4]$$

Of course, a difference between the definitions [2] and [4] can be only felt for aggregates containing very few spheres. Equation [4] will be used throughout this paper as a more physical definition, because it yields equality of gyration and spherule radius in the limit $N = 1$ (as for a "hollow" particle with its mass concentrated at the outer radius), whereas the gyration radius for one sphere, formally calculated using Eq. [2], is zero.

Besides the scaling law [1], the morphology of the fractal-like aggregates is characterized by the two-point density–density correlation function:

$$C(\mathbf{r}) \equiv \langle\langle \rho(\mathbf{r}_0)\rho(\mathbf{r}_0 + \mathbf{r}) \rangle\rangle_{|\mathbf{r}|=r}, \qquad [5]$$

where the brackets $\langle\langle \cdots \rangle\rangle$ represent the double average for all origins ($\mathbf{r}_0$) and orientations, and ρ is a "density" (unity inside a spherule and zero outside). In the case of fractal-like aggregates, $C(r)$ must have the form (7)

$$C(r) = A_c r^{D_f - d}, \qquad [6]$$

where A_c is a constant parameter, d is the Euclidean dimension of the physical space, and the exponent D_f is the same as in the scaling law [1].

Because of the finite size of fractal-like aggregates, the general form of the complete correlation function is more complicated than that given by Eq. [6]. Accounting for statistical invariance with respect to a change of length scale, the correlation function $C(r)$ can be rewritten as

$$C(r) = \hat{A}_c \left(\frac{r}{R_g} \right)^{D_f - d} f_c \left(\frac{r}{R_g} \right), \qquad [7]$$

where f_c is a cutoff function and $\hat{A}_c$ is a normalization constant. Rigorous prediction of the physical properties of aggregated particles, such as light scattering and energy, mass, and momentum transfer to and from the carrier gas, which are strongly dependent on aggregate morphology, must be based on detailed calculation of these properties for a statistically representative ensemble of aggregate forms and subsequent averaging. However, the direct experimental determination of fractal-like aggregate structures is difficult and often involves interpretation of 2-dimensional (e.g., TEM) images, requiring additional assumptions (8–10) and leading to new uncertainties. For our present purposes, a more efficient way involves the numerical generation of fractal-like structures using algorithms imitating the formation of fractal geometries in nature. A good overview of pioneering fractal generation methods can be found in Ref. (11).

In general, these "mimicking" algorithms can be divided into particle–cluster aggregation (PCA) and cluster–cluster aggregation methods (CCA), depending on whether aggregation in the simulation occurs between isolated particles and clusters, or between clusters. These methods yield structures fulfilling the statistical scaling law [1], with fractal dimensions D_f around

2.5 and 1.8, respectively, the last value in agreement with experimental data (6, 8, 9). However, with one notable exception (12), little attention is commonly paid to equally important agreement between the prefactor value k_f for observed and numerically generated aggregates. A possible reason for this is that, in contrast to the fractal dimension D_f, the prefactor value is much more difficult to determine experimentally. For example, the values of k_f retrieved from light scattering experiments with soot by different authors differ by almost a factor of 2 (8).

To appreciate that the situation is still more complicated, recall that the scaling dependence [1] is statistical and fulfilled for average parameters. This means that even for aggregated aerosols with equal gyration radius, R_g, there is a distribution of actual number of spherules N_a centered at the mean value N according to the equation

$$N = \int_1^\infty F(R_g, D_f, k_f, N_a)\, dN_a, \qquad [8]$$

where F is the distribution function for the number of spherules in aggregates of gyration radius R_g. If this distribution is narrow, one can assume the scaling law [1] to be fulfilled for each aggregate; otherwise all physical properties will depend on the form, and particularly on the first few moments (with respect to N_a), of the distribution function F, which can be different for different conditions of aggregate generation in experiment and specific numerical generation method. Currently, no "data" are available on comparisons of the distribution function F in experiments and various numerical generation algorithms. Nevertheless, meaningful calculations of fractal aggregate properties are still possible using so-called tunable numerical generation methods, such as the algorithms of Refs. (4, 13, 14), which yield structures with arbitrary prescribed fractal dimension *and* prefactor values. In contrast to the already mentioned "mimicking" algorithms, these methods are based on the assumption that the scaling dependence [1] is fulfilled exactly for each aggregate size, which is equivalent to zero width of the distribution function F, i.e.,

$$F = \delta\left[N_a - k_f\left(\frac{R_g}{a}\right)^{D_f}\right], \qquad [9]$$

where δ is the Dirac delta function. Tunable methods can be also used for simulating fractal aggregate populations with distribution functions F having nonzero width. This can be achieved, for example, by generating mixtures of structures exactly satisfying the scaling law with varying prefactors $k_f + \Delta k_f$ so that the average value of Δk_f is zero. The resulting aggregate population will satisfy the scaling law [1] with prefactor k_f on the average.

In this paper, a new variant of the sequential algorithm similar to that of Mackowski (4) is described in detail. A generalization of the tunable cluster–cluster aggregation (CCA) method of Thouy and Jullien (14) is also given. In the rest of the paper, these methods are used to numerically generate fractal-like aggregates with "narrow" distributions [9] for calculating the scaling laws for light scattering and energy and mass transfer to and from fractal aggregates in the free-molecular and continuum regimes.

2.1. Sequential Algorithm (SA)

This algorithm, which will be hereafter called sequential (SA), is a tunable particle–cluster aggregation method, where identical spherical particles are added iteratively, one by one. Here, the principal difference from the mimicking algorithms is that the scaling law [1] is fulfilled exactly at each step for prescribed values of fractal dimension and prefactor. Suppose that we have already built an aggregate of $N-1$ spherules. Combining the definition of the gyration radius [4] with the scaling law [1] for steps $N-1$ and N, it can be found that the center $\mathbf{r}_N$ of the next spherule must be situated on the surface of a sphere determined by the equation

$$\left(\mathbf{r}_N - \mathbf{r}^0_{N-1}\right)^2 = \frac{N^2a^2}{N-1}\left(\frac{N}{k_f}\right)^{2/D_f} - \frac{Na^2}{N-1} - Na^2\left(\frac{N-1}{k_f}\right)^{2/D_f}, \qquad [10]$$

where $\mathbf{r}^0_{N-1}$ is the center of mass of the first $N-1$ spherules (see Appendix). As soon as the new spherule is placed randomly at the surface of the sphere [10] with restrictions of not overlapping and having at least one contact point with the previously attached $N-1$ spherules, the procedure repeats for the next attaching spherule. At each intermediate step, the scaling law [1] is fulfilled exactly. A similar algorithm has been described by Mackowski (4), but the restriction [10] has not been formally given.

Figure 1 shows a cluster of 724 particles generated using the described algorithm. The fractal dimension and prefactor values were set to $D_f = 1.8$ and $k_f = 1.3$, respectively, which are the parameters reported by Cai *et al.* (15) for soot aggregates. The method produces highly ramified structures, with many "filaments" and certain symmetry (there is an obvious preferential direction), not very much resembling typical soot agglomerates observed on TEM photographs (8, 10, 16). For a more detailed characterization of aggregate morphology, the two-point correlation function [5] has been computed by generating a set of N_{ag} aggregates and consequent averaging:

$$C(r) = \frac{1}{N_{ag}}\sum_{i=1}^{N_{ag}}\left[\frac{n_i(r)}{4\pi r^2 h N}\right], \qquad [11]$$

where $n_i(r)$ is the number density of couples of particles lying at a distance $(r - h/2, r + h/2)$ and N is the total number of spherules in each aggregate. The normalization of the correlation

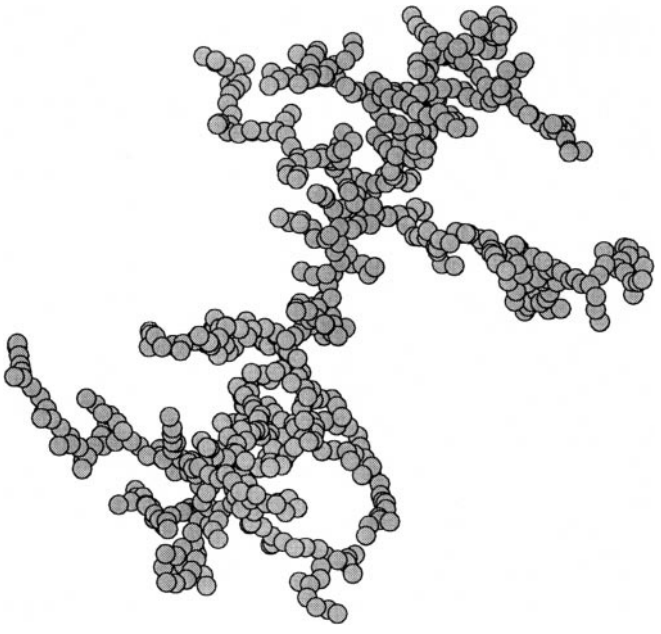

FIG. 1. A fractal-like aggregate of 724 spheres with fractal dimension $D_f = 1.8$ and prefactor $k_f = 1.3$ generated by a sequential algorithm (SA).

function is chosen to satisfy the following equation (17):

$$\int_0^\infty C(r) 4\pi r^2 \, dr = \frac{N-1}{2}. \qquad [12]$$

The dashed line in Fig. 2 shows the correlation function for SA-generated clusters, averaged over 40 aggregates of 2048 particles with fractal dimension $D_f = 1.8$ and fractal prefactor $k_f = 2.3$. Due to different behavior of correlations at different length scales, three zones can be distinguished in the plot:

(I) In the short range of distances, many discontinuities can be observed. We can appreciate a peak of the distribution function at $r/a = 2$, which is due to the fact that there is always a finite probability for a particle–particle distance $r = 2a$. An explanation for the discontinuity at $r/a_0 = 4$ can also be found in Ref. (17).

(II) For larger distances, say $r/a_0 > 5$, the distribution function follows a power law of the type given by Eq. [6], so that an exponent D_f characterizes the slope of this linear (in log–log scales) part of the graph.

(III) In the third zone, finite size effects of the aggregate result in a sharp decay of the correlation function.

It appears that for the SA aggregates, the calculated slope of the correlation function corresponds to a fractal exponent (2.08 ± 0.01) in Eq. [6], which is 15% higher than the fractal dimension of 1.8 exactly appearing in the scaling law [1]. The same discrepancy between the fractal dimension retrieved from the slope of the correlation function and the exponent of the scaling law [1] is illustrated by Fig. 3. It shows the dependence of the normalized correlation function $C(r)R_g^{3-D_f}$ on the normalized argument r/R_g calculated for 40 sequences of SA-generated aggregates with fractal dimension $D_f = 1.8$, fractal prefactor $k_f = 2.3$, and spherule number between 120 and 2000. The collapse into one curve of normalized correlation functions for different aggregate sizes is the result of the scaling invariance described by Eq. [7].

This contradiction is a significant drawback of the SA method which, as will be shown, can lead to systematic errors in the calculation of the physical properties for simulated aggregate structures. We can therefore conclude that for SA-generated aggregates different scaling laws exist for describing interparticle distances and fractal size. Such aggregates cannot be fully considered to be fractal-like objects.

2.2. *Tunable Cluster–Cluster Aggregation Algorithm (CCA)*

Thouy and Jullien (14) have developed a so-called tunable cluster–cluster aggregation (CCA) algorithm, based on a

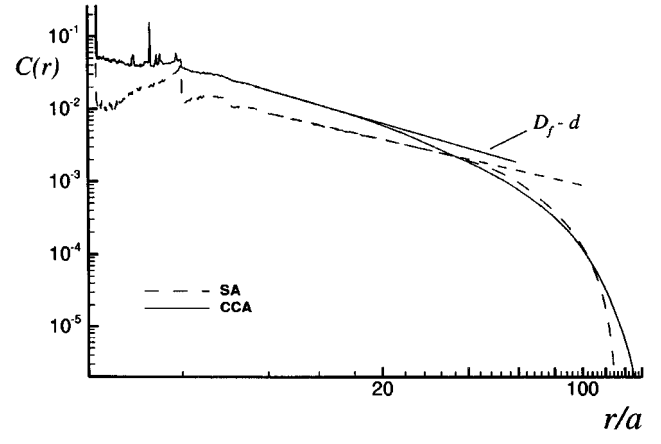

FIG. 2. Correlation function for numerically generated aggregates with fractal dimension $D_f = 1.78$ and prefactor $k_f = 2.3$, averaged over 40 clusters of $N = 2048$ particles. Unlike the slope for the SA curve, the slope for the CCA aggregates agrees with the prescribed fractal dimension.

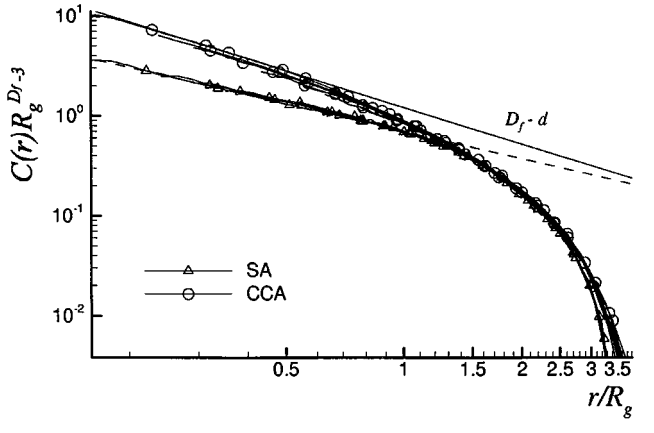

FIG. 3. Collapse of the scaled correlation functions for cluster sizes in the range $N = 120$–2000. The slope of the CCA aggregates (shown by the solid line) agrees with the fractal dimension, whereas the slope for the SA aggregates does not (dashed line).

hierarchical scheme of aggregation of equal-sized clusters on each step and resulting in fractal-like agglomerates exactly satisfying the scaling law [1]. In the present paper, a slightly more general algorithm will be introduced, which does not preclude agglomeration of clusters with equal number of spherules, so that their number in the final aggregate is not necessarily a power of 2.

For any two aggregates containing N_1 and N_2 equally sized spherules and having the gyration radii R_1 and R_2, respectively, the following equation, resulting from the definition [4] of gyration radius (or from the more commonly used definition [2]), is always valid:

$$(N_1 + N_2)R_g^2 = N_1R_1^2 + N_2R_2^2 + \frac{N_1N_2}{N_1 + N_2}\Gamma^2, \qquad [13]$$

where Γ is the distance between the geometrical centers of the two clusters and R_g is the gyration radius of their combination. A detailed derivation of the equation is given in the Appendix. Equation [13] yields a necessary and sufficient condition for exact fulfillment of the scaling law [1] by the resulting cluster:

$$\Gamma^2 = \frac{a^2(N_1 + N_2)}{(N_1N_2)}\left(\frac{N_1 + N_2}{k_f}\right)^{2/D_f} - \frac{N_1 + N_2}{N_2}R_1^2 - \frac{N_1 + N_2}{N_1}R_2^2. \qquad [14]$$

Based on this equation, the CCA algorithm starts with SA-generated clusters of very few, 5–8, spherules with prescribed values of D_f and k_f and then combines them pairwise, following a hierarchical scheme. Each of the agglomeration events includes placing the geometrical centers of two clusters to random points at a distance given by Eq. [14] and their rotation (as solid bodies) until the combining clusters have at least one contact point and no overlapping. After performing the procedure for all clusters on one level, another level involving larger clusters starts, etc. The final result is one large cluster, satisfying the scaling law [1] exactly.

Figure 4 shows an aggregate of 724 spherules generated with this algorithm. In contrast to SA-generated structures, no central part or symmetry of the aggregate can be noticed, and it looks similar to aggregates obtained by "mimicking" CCA algorithms and resembles the agglomerates produced by gas-phase synthesis and soot clusters. However, a more detailed structural analysis reveals the following main advantage of the CCA algorithm over the SA method:

It has been found that the slope of the correlation function of the CCA-generated aggregates agrees, to rather high accuracy, with the value $3 - D_f$ corresponding to the prescribed fractal dimension. For example, the solid line in Fig. 2 shows the averaged (over 40 samples) correlation function for 2000 particles generated by the tunable CCA method with fractal dimension $D_f = 1.8$ and fractal prefactor $k_f = 2.3$. The slope of the linear (in the log–log scale) part of the graph is only 1% different from the expected value 1.2. Similar agreement has been observed for

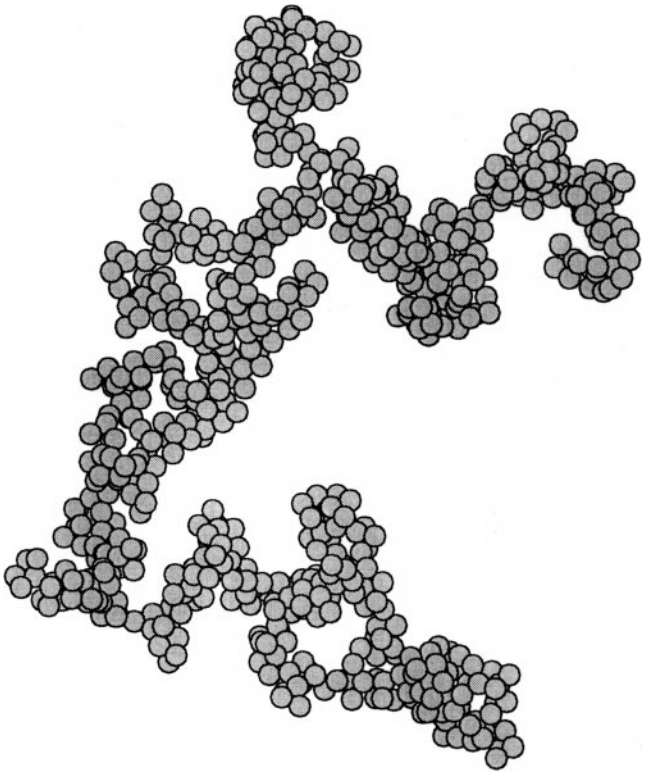

FIG. 4. An aggregate of 724 particles with fractal dimension $D = 1.8$ and prefactor $k_f = 2.3$ generated using the tunable CCA algorithm.

the normalized correlation function calculated for clusters containing between 100 and 2000 spherules, shown by solid lines in Fig. 3. Our calculations with a number of CCA clusters with various fractal dimensions between 1 and 3 and different prefactor values show that this is a general feature of the CCA algorithm and encourage its use for modeling physical properties of natural fractal-like aggregates. Finally, the effect of increasing the number of spherules in the correlation function can be observed in Fig. 5.

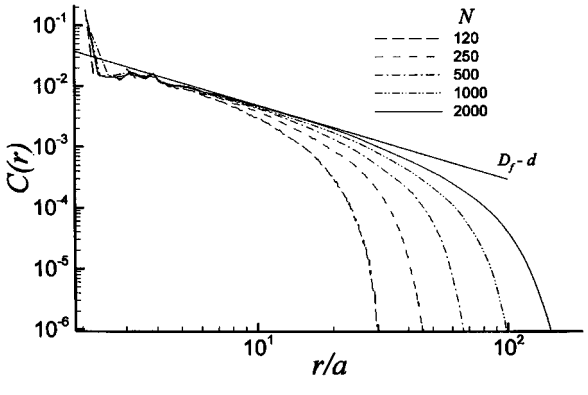

FIG. 5. Correlation function for CCA aggregates with fractal dimension 1.8 and prefactor 2.3, averaged over 20 clusters, in the size range $N = 120$–2000. Also shown is the theoretical slope.

3. LIGHT SCATTERING

One of the main goals of the present paper is to understand the difference in simulations of light scattering which can be expected in application of the two described methods of aggregate numerical generation. Light scattering and absorption properties of fractal-like aggregates, as well as the vast literature on the topic, have been recently reviewed in detail by Sorensen (18). It can be noticed that the optical properties of fractal-like aggregates are determined mainly by the correlation function [7]. Indeed, the scattered intensity in a small-angle scattering experiment on aggregates of N identical spheres can be expressed as

$$I(\mathbf{q}) = NS(\mathbf{q})P(\mathbf{q}), \quad [15]$$

$$\mathbf{q} = \mathbf{k}_s - \mathbf{k}_i, \quad [16]$$

$$|\mathbf{q}| = \frac{4\pi}{\lambda}\sin\frac{\theta}{2}, \quad [17]$$

where $P(\mathbf{q})$ is the scattering intensity of an isolated sphere, $S(\mathbf{q})$ is the scattering function or structure factor, $\mathbf{q}$ is the scattering vector, λ is the wavelength, θ is the scattering angle, and $\mathbf{k}_s$ and $\mathbf{k}_i$ are the scattered and incident wave vectors, respectively. Within the framework of Rayleigh–Debye–Gans (RDG) theory (19), the clusters are assumed to consist of identical and independent scattering spheres and the scattering function is a Fourier transform of the above-mentioned density correlation function:

$$S(\mathbf{q}) = \frac{1}{N}\sum_{i,j} e^{i\mathbf{q}\cdot\mathbf{r}_{ij}} = 2\int_0^\infty e^{i\mathbf{q}\cdot\mathbf{r}} C(\mathbf{r})\, d\mathbf{r}, \quad [18]$$

where, according to Eq. [12], the correlation function C must account for one additional pair with $i = j$ (or $\mathbf{r} = 0$). It should be noticed that Mackowski (4) has developed a rigorous multipole expansion theory for an accurate calculation of light scattering and absorption by aggregates, which, however, does not yield a simple relation between the scattering and the correlation function. In many practically important situations, when multiple scattering is negligible and the Rayleigh limit conditions are fulfilled, Mackowski's theory (4) can be reduced to the RDG approach.

Averaged over all possible directions of the scattering vector, the structure factor depends only on its magnitude [17]:

$$S(q) = 2\int_0^\infty \frac{\sin(qr)}{q} 4\pi r C(r)\, dr. \quad [19]$$

If the correlation function were a simple power law [6], the Fourier transform [19] would also yield the structure factor as a power function of q with exponent $-D_f$. However, due to the finite size of the aggregates, the correlation function is always modulated by the cutoff function, shown in Eq. [7]. An asymptotic analysis of the Fourier transform [19] yields the following behavior for the structure factor, depending on the value of the product qR_g (11):

$$qR_g \lesssim 1: \quad S(qR_g) = N\left(1 - \frac{1}{3}\frac{q^2R_g^2}{3}\right), \quad [20]$$

$$1 < qR_g: \quad S(qR_g) = C_l q^{-D_f}, \quad [21]$$

for the so-called Guinier and power-law regimes, respectively. The cutoff function determines the value of the constant C_l and also the region where the power-law approximation [21] becomes valid. Besides that, due to the already mentioned singularity of the correlation function at $r = 2a$ (each spherule must have at least one neighbor at this distance), the structure factor for large q must tend to

$$S_{2a} = 1 + C_a\frac{\sin(2aq)}{q}, \quad [22]$$

where C_a is a constant related to the coordination number for $r = 2a$, as discussed by Hasmy *et al.* (17). This is the cause for the oscillations detectable at large enough values of qR_g. Equations [19]–[22] are a starting point for the optical characterization of the fractal aggregate morphology by measuring the angular dependence of the intensity of the scattered light (20).

Equation [19] was used to calculate the structure factor for aggregates containing 2000 particles, generated numerically using the described SA and CCA algorithms with fractal dimension 1.78 and prefactor 2.3. Our results are shown in Fig. 6, where the structure factor is plotted as a function of the product qR_g and all three regimes [20]–[22] can be observed. The structure factor for CCA aggregates, shown by a solid line, satisfies the power law [21], with the expected exponent $-D_f$ in an interval immediately after the Guinier regime, but later the discrepancy increases and the oscillations [22] can be seen. The extent of the

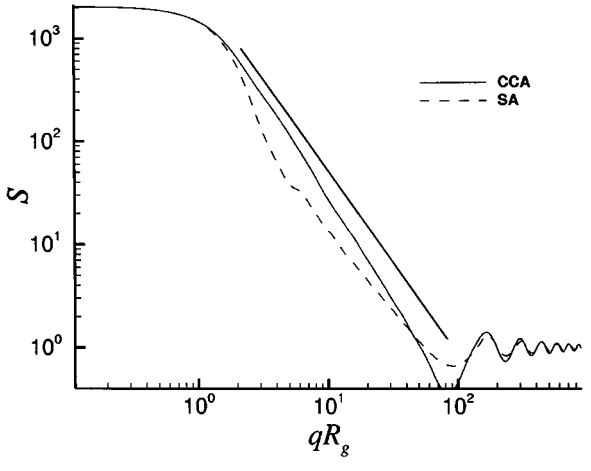

FIG. 6. Structure factor (scattering function) for fractal-like aggregates generated using different algorithms. The solid straight line has slope $-D_f$.

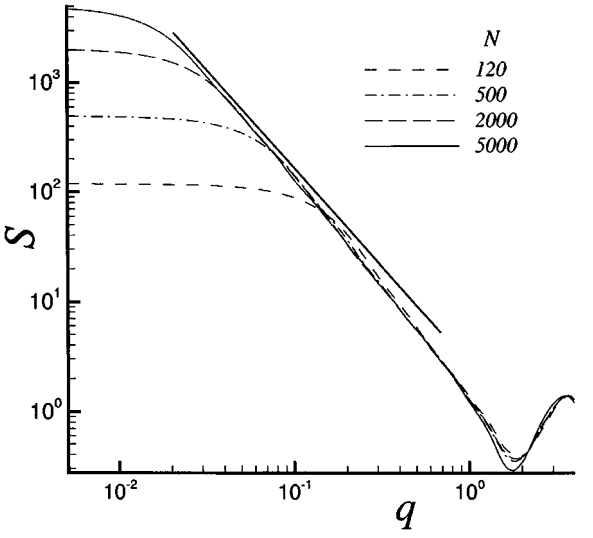

FIG. 7. Scattering function for CCA-generated aggregates, showing the increase in the linear range given by Eq. [21] with aggregate size. The solid straight line has the expected slope $-D_f$.

power-law interval increases with the size of the aggregates, as shown in Fig. 7 for CCA-generated aggregates with sizes between 120 and 5000. For small enough aggregates, the determination of the fractal dimension from light scattering experiments alone can become problematic.

As expected, the structure factor for SA-generated aggregates, shown by a dashed line in Fig. 6, reveals the power-law behavior with an exponent corresponding to the exponent of its correlation function, rather than to the scaling exponent in Eq. [1]. After the initial power-law interval, the line breaks and another nearly linear (in log–log scales) segment of the curve with a lower slope can be observed. It is interesting that a very similar behavior of the structure function has been found by Oh and Sorensen (21) for fractal-like aggregates generated using a "mimicking" diffusion-limited aggregation (DLA) algorithm. In their case, the slopes of both power-law intervals conflicted with the value 2.5 of the scaling exponent, revealing non-self-similarity of the generated structures.

4. ENERGY AND MASS TRANSFER

4.1. Free Molecular Regime Calculations

Now, the effect of aggregate morphology on its *transport properties* can be investigated. However, a rigorous calculation of energy and mass tranfer to and from multisphere clusters requires the application of more advanced theoretical methods than the RDG approach used for light scattering problems.

Consider the energy transfer between an aggregate of N motionless spherical particles (spherules) at temperature T_p and a gas at temperature T_g when the mean free path of the gas molecules is much larger than the spherule radius, so that the intermolecular collisions can be neglected. The rate of aggregate–gas energy transfer is given by the equation

$$\dot{Q}_i - \dot{Q}_r = \int_{\mathbf{v}\cdot\mathbf{n}<0}\int_{S_a}\left[\frac{1}{2}mv^2+\varepsilon_i\right]\mathbf{v}\cdot\mathbf{n}\,f_i\,d^3v\,dS - \int_{\mathbf{v}\cdot\mathbf{n}>0}\int_{S_a}\left[\frac{1}{2}mv^2+\varepsilon_r\right]\mathbf{v}\cdot\mathbf{n}\,f_r\,d^3v\,dS, \quad [23]$$

where m is the mass of the gas molecules, S_a the surface of the aggregate, $\mathbf{v}$ the gas molecule velocity, and f the velocity distribution function. The subscripts i and r refer to incident and reflected conditions, respectively, while the terms $\varepsilon_{i,r}$ account for the energy associated with internal (e.g., vibrational and rotational) degrees of freedom of the gas molecules. In the case of monatomic gas without electronic excitation, the mass transfer of molecules to an absorbing aggregate can be modeled using the same scheme, by assigning α the meaning of the absorption probability per impact. Indeed, within the described scheme of the energy transfer, only the first collisions resulting in accommodation of energy are important because all parts of the aggregate will be assumed here to have the same temperature. The following motion of a simulated molecule does not influence the energy transfer balance, even if multiple molecule–particle collisions take place. In the absorption simulation, too, only the first "absorbing" collision is important, whereas the laws of motion and reflection at the walls are identical for both transfer processes. Therefore, one calculation yields both the energy transfer and molecule absorption rates for an aggregate.

The conventional approach to the solution of these problems would be the application of the Monte Carlo (MC) method (22). This method is based on simulation of the trajectories of individual molecules and calculation of the energy transfer at each of the molecule–particle collisions. In the MC approach, the initial velocities of the simulated molecules are chosen randomly, corresponding to a Maxwellian distribution at the ambient gas temperature. At each collision, the molecule is specularly reflected with a probability $(1-\alpha)$, or diffusely scattered with probability α, where α is the translational energy accommodation coefficient. The energy transferred at each simulated molecule–particle collision can be calculated from the difference between the translational (and internal) energy of the molecule before and after collision. By repeating these calculations many times and averaging the result, the energy transfer rate corresponding to a given particle–gas temperature difference can be evaluated.

Relatively recently (23), it has been found that such MC procedures can be dramatically accelerated by using so-called quasi-random sequences instead of conventional pseudorandom numbers. In our algorithm, Halton sequences have been implemented (24). The nth term of the Halton sequence based on prime p is generated as

$$z_n = \frac{a_0}{p} + \frac{a_1}{p^2} + \cdots + \frac{a_m}{p^{m+1}}, \quad [24]$$

where a_i are the integers from the base p expansion of n; that is,

$$[n]_p = a_{m+1}a_m \cdots a_2a_1a_0. \quad [25]$$

For example, for $p = 2$, the binary representation of $n = 5$ is $[5]_2 = 101$, giving $a_0 = 1$, $a_1 = 0$, and $a_2 = 1$, and the corresponding term of the Halton sequence is $z_5 = 0.625$.

Quasi-Monte Carlo (QMC) algorithms, based on the use of quasi-random sequences, have much better performance compared to the MC algorithms. For example, estimated errors using pseudorandom sequences in the MC approach are of order $O(1/L^{1/2})$, where L is the number of simulated particle trajectories, while the errors in the QMC methods decrease much faster, in some cases like $O(1/L)$. We tested both methods on the known solution of heat transfer rate for an isolated, motionless sphere, where the ratio T_g/T_p is near unity; i.e.,

$$\dot{Q} = \frac{1}{2}\alpha\pi a^2 p_g \bar{c}\left(\frac{\gamma+1}{\gamma-1}\right)\left(\frac{T_g}{T_p} - 1\right), \quad [26]$$

where a is the sphere radius, P_g is the gas pressure, $\bar{c}$ is the mean molecular thermal speed, and γ is the gas specific heat ratio, or 5/3 for monatomic gases in their ground electronic states. Here, we neglect the possible variation of the adiabatic specific heat ratio, which can happen at high particle–gas temperature differences (25). Figure 8 shows the results of these calculations for a case of complete accommodation on the particle surface, giving the average MC error proportional to $N^{-0.49}$, while the corresponding QMC error decreased as $N^{-0.72}$.

The described QMC approach has been applied here to calculate the particle–gas energy transfer rates for the numerically generated fractal-like aggregates depicted in the previous sections. In all cases, we have considered a monatomic gas with molecules possessing only translational kinetic energy.

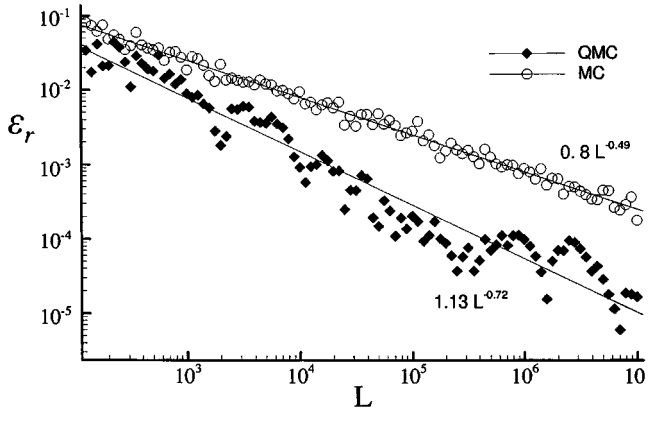

FIG. 8. Relative error ε_r for Monte Carlo and quasi-Monte Carlo calculations of the heat transfer rate to one sphere.

4.2. Continuum Regime

In the continuum regime, many of the required aggregate physical properties can be found from the solution of the external Dirichlet problem:

$$\Delta\Phi = 0, \quad [27]$$

$$r_i = a_i: \quad \Phi = \Phi_i; \quad r_i \to \infty: \quad \Phi \to \Phi_\infty, \quad [28]$$

where Δ is the Laplacian (∇^2) differential operator, Φ is a scalar potential with fixed values Φ_i and Φ_∞ on the surface of a sphere i and at infinity, respectively, and r_i is the distance from the center of the sphere i. After solving the external boundary problem [27]–[28], the corresponding fluxes can be found by integration over the aggregate surface:

$$\dot{Q} = \sum_{i=1}^{N} \dot{Q}_i, \quad [29]$$

$$\dot{Q}_i = -\int_{S_i} k_g \frac{\partial\Phi}{\partial r_i}\, ds_i, \quad [30]$$

where k_g is the transfer coefficient for the corresponding property. Examples of the mathematically equivalent problems which can be reduced to solution of Eqs. [27]–[30] include the calculation of

aggregate–gas *heat transfer rate*: $\Phi = T$ is the gas temperature and k_g is the heat conductivity coefficient of the carrier gas, here considered constant

absorption rate: $\Phi = c$ is the concentration of species diffusing to the absorbing aggregate surface and k_g is the Fick diffusivity of the species

electric capacitance of the conducting aggregate: Φ is the electrostatic potential, and $k_g = \varepsilon_g$ is the dielectric constant of the gas

An efficient method, which will be used for solution of the Dirichlet and similar problems for a set of arbitrary spheres, involves a multipole expansion of the potential in a series of spherical harmonics. Originally, it was developed to calculate the scattering of electromagnetic waves by a cluster of spheres (26) and later applied to predict light absorption/scattering by N-sphere aggregates (4) as well as hydrodynamic (27) and thermophoretic (28) behavior of two-sphere aggregates. Using the notations of Mackowski (4), the scalar potential Φ is written in the form

$$\Phi = \Phi_\infty + \sum_{j=1}^{N}\sum_{n=0}^{\infty}\sum_{m=-n}^{n} a_{mn}^{j} u_{mn}^{j-}(r_j, \theta_j, \varphi_j), \quad [31]$$

$$u_{mn}^{j-} = \frac{1}{r_j^{n+1}} P_n^m(\cos\theta_j)\exp(im\varphi_j), \quad [32]$$

where u_{mn}^{j-}, r_j, θ_j, and φ_j are solid spherical harmonics of order n and spherical coordinates centered about the sphere j, P_n^m is the associated Legendre function, and a_{mn}^j are the expansion coefficients. According to the addition theorem (29), the spherical harmonics centered at sphere j can be expressed in terms of the spherical harmonics centered at any other sphere i:

$$u_{mn}^{j-}(r_j, \theta_j, \varphi_j) = \sum_{l=0}^{\infty} C_{mnkl}^{ij} u_{mn}^{i+}(r_i, \theta_i, \varphi_i), \quad [33]$$

$$u_{kl}^{i+} = r_i^l P_l^k(\cos\theta_i) \exp(im\varphi_i), \quad [34]$$

where the transformation matrix C_{mnkl}^{ij} depends solely on the mutual position of the ith and jth particles. Combining Eqs. [28] and [31]–[33] and neglecting the spherical harmonics of the order higher than L, we obtain the linear system of $N \times L \times (L+2)$ equations:

$$a_{mn}^i + (a_i)^{2n+1} \sum_{j \neq i}^{N} \sum_{l=0}^{L} \sum_{k=-l}^{l} C_{klmn}^{ij} a_{kl}^j = a_i(\Phi_i - \Phi_\infty)\delta_n^0, \quad [35]$$

where δ_n^0 is the Kronecker delta and a_i is the radius of the sphere i. By solving the linear system [35], a distribution of potential can be found with any desirable accuracy, controlled by the truncation level L. The transfer rates to individual spherules can be expressed directly in terms of the expansion coefficients a_{00}^i:

$$\dot{Q}_i = 4\pi k_g a_{00}^i. \quad [36]$$

It was found that very good accuracy can be achieved already at the truncation level of $L = 2$, so $L = 3$ was chosen for all calculations discussed in the following section.

For an isolated sphere, Eqs. [35] and [36] yield a classical equation for a transfer rate to a single particle:

$$\dot{Q}_1 = 4\pi k_g a(\Phi_1 - \Phi_\infty). \quad [37]$$

4.3. Results and Discussion

Transfer rates for fractal-like aggregates have been determined using the described algorithms for generation of the aggregate morphology and calculation of their physical properties. Because of the mentioned similarity in the calculation of the energy and mass transfer rates in both the free-molecular and continuum regimes, the results are explicitly presented for the energy transfer problem, without loss of generality. It is assumed that the particle clusters consist of N touching isothermal spheres of identical size and physical properties.

Figure 9 shows the free-molecular heat transfer distribution within the particles for a CCA-generated aggregate containing 100 spherical particles in the case of complete accommodation. The intensity of gray shows the magnitude of the energy transfer rate in multiples of the transfer rate [26] for a single isolated sphere under the same ambient gas conditions. A small difference in the energy transfer values for different spherules corresponds to a weak shielding effect, characteristic for transport processes in the free-molecular regime. For small, but finite values of α, the shielding effect is still less pronounced than for the same aggregate under complete accommodation conditions, as can be seen in Fig. 10.

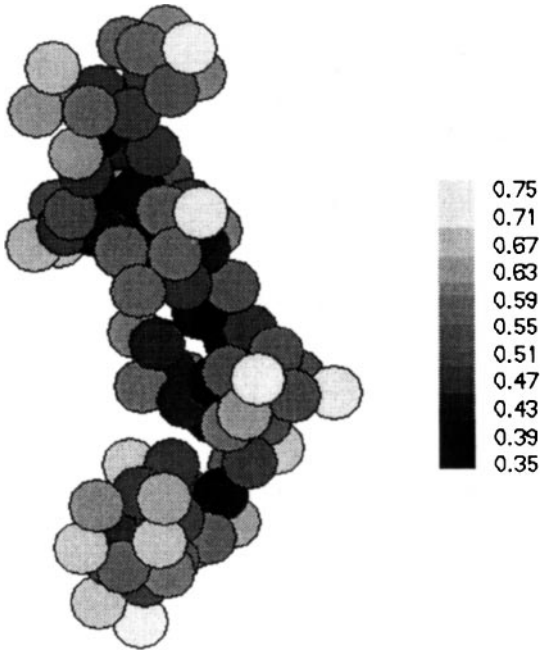

FIG. 9. Heat transfer rates to and from 100 aggregated spherules (fractal dimension is 1.8 and prefactor is 2.3) in the free-molecular regime with complete accommodation. The data are normalized by the heat transfer rate to an isolated spherule under the same conditions.

Quantitatively, the overall shielding effect can be characterized by the ratio of the total heat transfer to the aggregate to the product of spherule number and the transfer rate to an isolated spherule in the same environment:

$$\eta \equiv \frac{\dot{Q}}{N\dot{Q}_1}. \quad [38]$$

In the limit $\alpha \to 0$, the molecule kinetic energy, on average, changes negligibly at each collision with the aggregate and all parts of the aggregate become equally accessible to the energy transfer so that it is unity regardless of aggregate form and size. With increase of the accommodation coefficient, the shielding factor η decreases, as shown in Fig. 11. Points on three curves in Fig. 11 show the average values of η calculated for 30 CCA-generated aggregates with fractal dimension 1.8 and prefactor 2.3, containing 5, 100, and 500 spherules, respectively. As could be expected, the decrease is faster for larger aggregates, displaying a stronger shielding effect.

Figure 12 shows the corresponding continuum-regime distribution of energy transfer rates to a fractal-like aggregate in

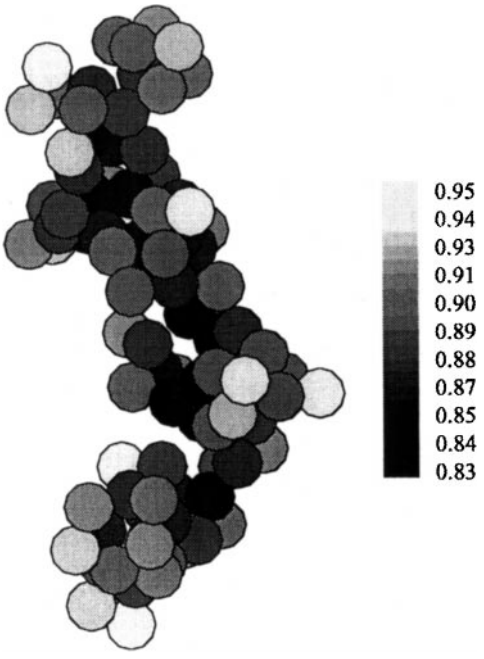

FIG. 10. Distribution of the heat transfer rates for the same aggregate, but with the surface accommodation coefficient $\alpha = 0.1$ in the free-molecular regime.

multiples of the transfer rate [37] to an isolated spherule. In contrast to the free-molecular regime illustrated for the same aggregate by Fig. 9, the shielding effect in this limit is much more pronounced, so that the values of the transfer rates to the perimeter spheres can be over an order of magnitude higher than that for the core spherules.

The aggregate–gas energy transfer rates have been calculated for fractal-like aggregates with different prefactors, fractal dimensions, and sizes and expressed in terms of the equivalent effective heat transfer radius R_{eff} for the free-molecular and continuum regimes, defined respectively by

$$\dot{Q}_{fm} \equiv \frac{1}{2}\alpha\pi R_{eff}^2 p_g \bar{c}\left(\frac{\gamma+1}{\gamma-1}\right)\left(\frac{T_g}{T_p}-1\right) \qquad [39]$$

and

$$\dot{Q}_c \equiv 4\pi k_g R_{eff}(\Phi_1 - \Phi_\infty). \qquad [40]$$

Thus, R_{eff} can be regarded as the radius of a single solid sphere with the same energy transfer rate as an isothermal aggregate under identical conditions.

In the case of complete accommodation on the surface, the equivalent radius R_{eff} is determined only by the geometry of the aggregate and, depending on the application, is called the heat transfer radius or diffusion radius. It is often difficult even to roughly estimate the value of the equivalent radius of an irregularly shaped aggregate, and here accurate calculations for

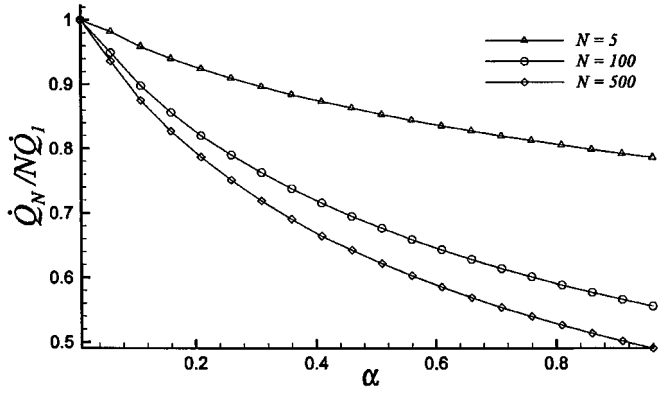

FIG. 11. Total heat/mass transfer rate to/from fractal-like aggregates with $D_f = 1.8$ and $k_f = 2.3$. The data are normalized by a sum of rates to N isolated spheres under the same conditions.

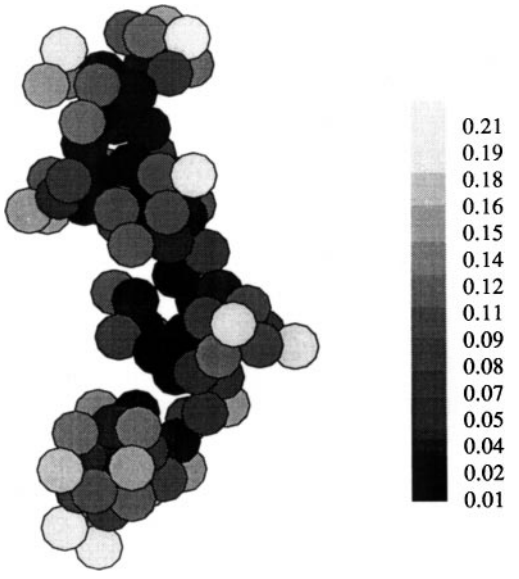

FIG. 12. Distribution of the continuum-regime heat transfer rates for the aggregate shown in Figs. 9 and 10, in units of the heat transfer to an isolated spherule.

TABLE 1
Calculated Exponents D_h for Aggregates with Different Prefactor and Fractal Dimension Values in the Free-Molecular Regime

k_f	$D_f = 1.3$	$D_f = 1.78$	$D_f = 2.3$	Generation method
1.3	2.04	2.14	2.36	CCA
	2.07	2.09	2.27	SA
2.3	2.06	2.2	—[a]	CCA
	2.05	2.07	2.31	SA

[a] Aggregates with fractal dimension 2.3 and prefactor 2.3 could not be produced by the CCA algorithm.

TABLE 2
Calculated Exponents D_h for Aggregates with Different Prefactor and Fractal Dimension Values in the Continuum Regime

k_f	$D_f = 1.3$	$D_f = 1.78$	$D_f = 2.3$	Generation method
1.3	1.52	1.93	2.35	CCA
	1.59	1.85	2.23	SA
2.3	1.65	2.07	—[a]	CCA
	1.65	1.88	2.31	SA

[a] Aggregates with fractal dimension 2.3 and prefactor 2.3 could not be produced by the CCA algorithm.

TABLE 4
Calculated Prefactors k_h for Aggregates with Different Prefactor and Fractal Dimension Values in the Continuum Regime

k_f	$D_f = 1.3$	$D_f = 1.78$	$D_f = 2.3$	Generation method
1.3	1.56	1.16	0.89	CCA
	1.46	1.29	1.06	SA
2.3	1.68	1.32	—[a]	CCA
	1.67	1.63	1.34	SA

[a] Aggregates with fractal dimension 2.3 and prefactor 2.3 could not be produced by the CCA algorithm.

various cluster geometries can establish characteristic dependencies, which can be easily applied in engineering practice. The calculations with the same values of parameters N, D_f, and k_f have been performed and averaged over 50 fractal-like numerically generated aggregates. It should be mentioned that the mass and energy transfer rates calculated for *individual* numerically generated aggregates in both the free-molecular and continuum regimes have been found to deviate by only a few percent from their average values.

These results indicate that the size dependencies of the aggregate equivalent radius satisfy the scaling law

$$N = k_h R_{eff}^{D_h}, \qquad [41]$$

where N is the number of particles of the aggregate, D_h is the scaling exponent, and k_h is the constant prefactor. Tables 1 and 2 give the calculated scaling exponents D_h for transfer processes in the free-molecular and continuum regimes, respectively, for aggregates generated using different algorithms with different fractal dimensions and prefactors. The difference between the scaling exponents D_h for numerically generated clusters built using the SA and CCA methods is of the same order of magnitude or smaller than the difference of the slopes of the corresponding scaled correlation functions shown in Fig. 3.

Significantly, for small fractal dimensions, the exponents D_f and D_h are different and there is no proportionality between the gyration and effective radius, whereas for fractal dimensions above 2 D_f and D_h are close and R_{eff} is proportional to R_g. This trend is much more evident in the continuum regime (Table 2) due to a more pronounced shielding effect.

As shown in Table 3, the prefactor k_h, defined by Eq. [41], is almost independent of the fractal dimension for free-molecular transfer processes, while the continuum regime calculations (Table 4) reveal significant decrease of k_h with fractal dimension. Qualitatively, these effects do not depend on the way the aggregates have been generated.

One of the widely used assumptions for calculating free-molecular heat transfer rate to and from a fractal-like aggregate involves completely neglecting the shielding effect for aggregates with fractal dimension below 2. Interpolating the dependence between D_f and D_h in the interval of fractal dimensions $2 < D_f < 3$, the following scaling has been suggested in Ref. (5):

$$D_f \le 2: \quad D_h = 2; \quad D_f > 2: \quad D_h = D_f. \qquad [42]$$

These formulae imply direct proportionality of the total energy transfer rate to the number of spherules N for loose aggregates with fractal dimension below 2 and a proportionality between the effective and gyration radii for dense aggregates with fractal dimensions higher than 2.

TABLE 3
Calculated Prefactors k_h for Aggregates with Different Prefactor and Fractal Dimension Values in the Free-Molecular Regime

k_f	$D_f = 1.3$	$D_f = 1.78$	$D_f = 2.3$	Generation method
1.3	1.15	1.1	0.95	CCA
	1.1	1.18	1.08	SA
2.3	1.22	1.2	—[a]	CCA
	1.23	1.4	1.32	SA

[a] Aggregates with fractal dimension 2.3 and prefactor 2.3 could not be produced by the CCA algorithm.

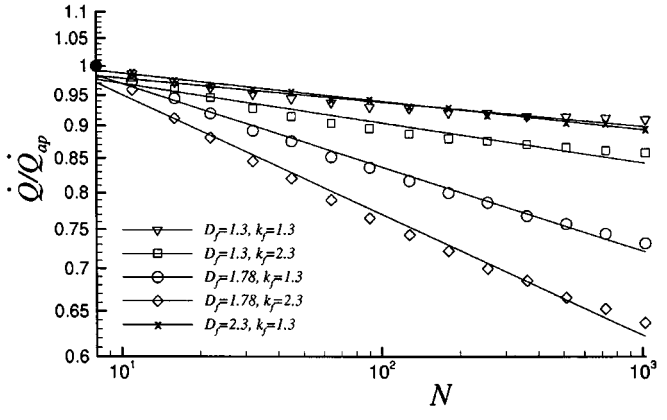

FIG. 13. Ratio of the calculated free-molecular regime energy transfer rate to the approximate transfer rate predicted by the scaling law [42] as a function of the spherule number of the aggregate for different values of the fractal dimension and prefactor.

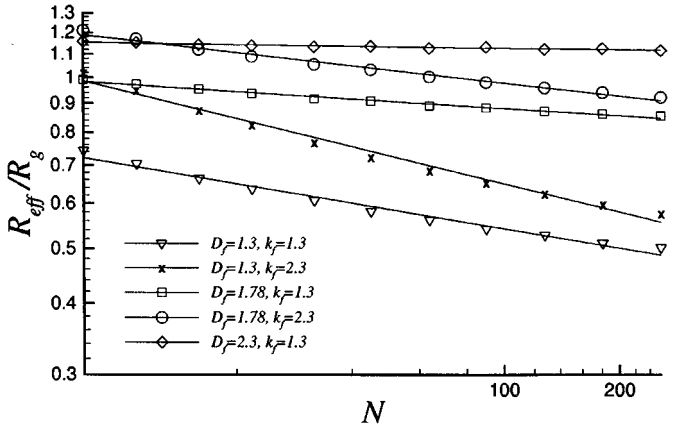

FIG. 14. Ratio of the calculated continuum regime energy transfer radius and the gyration radius as a function of the particle number in the numerically (CCA) generated fractal-like aggregates for different values of the fractal dimension and prefactor.

Figure 13 shows the ratio of the free-molecular energy transfer rates to those based on the scaling [42] assuming that they are equal for aggregates of 8 spherules. The aggregates were generated numerically, using the described CCA algorithm. Using log–log scales, the graphs are well approximated by straight lines, in agreement with the power laws [41]. These results show that the conjecture [42] can be used to estimate the energy transfer rate to and from fractal-like aggregates for fractal dimensions lower than 1.3 and higher than 2.3. However, for often encountered fractal dimensions around 1.8–2, the errors associated with the use of the scaling law [42] can be as high as 40%.

In the continuum regime, the equivalent heat or mass transfer radius is often assumed to coincide with the gyration radius; i.e.,

$$R_{eff} \approx R_g. \qquad [43]$$

The actual size dependencies of the ratio R_{eff}/R_g, calculated for CCA-generated aggregates with various fractal dimension and prefactor values, are shown in Fig. 14. Assumption [43] is seen to be justified only for dense fractal-like aggregates with fractal dimension above 2 and fails for smaller fractal dimensions. Using a multipole expansion method to calculate fluid dynamics in the vicinity of fractal-like aggregates, we have recently found a very similar behavior of the ratio of hydrodynamic radius and gyration radius (31).

5. CONCLUSIONS

The goal of this paper has been to establish the dependencies between the major physical properties of fractal-like aggregates and their size and structural parameters, such as fractal dimension and fractal prefactor. Since the structure of aerosol clusters in nature and industrial applications is different, two independent numerical algorithms for generation of aggregate geometry have been developed, which allow easy "tuning" of the structural parameters to prescribed values. It was found that the aggregates having the same structural parameters and close correlation functions also have close major physical properties regardless of possible differences in the appearance, which encourages the calculation of these properties for natural fractal-like aerosols using the simulated geometries.

In this work, the detailed study of the numerically generated aggregates based on calculation of the pair correlation function and its Fourier transform yielded (in the framework of widely used RDG theory) aggregate light scattering properties, important for practical *in situ* optical characterization of aerosol aggregates (20).

The energy transfer and mass transfer to and from aggregated aerosols in the free-molecular regime have been investigated using a quasi-Monte Carlo method, which, for the problems studied, was shown to be at least 100 times more efficient compared to conventionally used Monte Carlo techniques. The detailed calculation of the mass and energy transfer rates to ensembles of numerically generated random aggregates yielded the scaling dependencies of these properties. In the practically important region of fractal dimension near 2, the calculated scaling laws have been found to differ substantially from those often postulated in the literature.

Calculation of the same aggregate physical properties in the continuum regime involved the detailed solution of the Laplace equation, with the boundary conditions on the complicated surface of aggregates consisting of up to some hundreds of spherules. This problem has been efficiently solved using the multipole expansion of the scalar potentials in series of spherical harmonics with controllable accuracy. As in the case of free-molecular properties, calculations have been performed to sets of random aggregates having the same fractal dimension and prefactor values and later averaged to yield the reported scaling dependencies. In general, the common practice of using the gyration radius as a basis for calculating the required physical properties of fractal-like aggregates was found to be justified only for aggregates with fractal dimensions above 2.

The described rigorous methods will be used for developing accurate approximate formulae for transfer processes between particle clusters and the carrier gas as well as for testing accuracy of existing simplified models for these processes, such as the modified porous media approach (32).

APPENDIX: DERIVATION OF EQS. [10] AND [13]

Any aggregate of N spheres can be arbitrarily divided into two clusters containing N_1 and N_2 spheres, respectively, with geometrical centers $\mathbf{r}_0'$ and $\mathbf{r}_0''$:

$$\mathbf{r}_0' = \frac{1}{N_1}\sum_{k=1}^{N_1}\mathbf{r}_k, \qquad [A1]$$

$$\mathbf{r}_0'' = \frac{1}{N_2}\sum_{l=1}^{N_2}\mathbf{r}_l, \qquad [A2]$$

where the indices k and l are reserved to spherules belonging to different clusters. According to definitions [A1], [A2], and [3], the radius vectors of the aggregate center and both of its parts satisfy the equations

$$N\mathbf{r}_0 = N_1\mathbf{r}_0' + N_2\mathbf{r}_0'', \qquad [A3]$$

$$\mathbf{r}_0' - \mathbf{r}_0 = -\frac{N_2}{N}\mathbf{\Gamma}, \qquad [A4]$$

$$\mathbf{r}_0'' - \mathbf{r}_0 = \frac{N_1}{N}\mathbf{\Gamma}, \qquad [A5]$$

$$\mathbf{\Gamma} = \mathbf{r}_0'' - \mathbf{r}_0', \qquad [A6]$$

where $\mathbf{\Gamma}$ is the vector connecting the centers of two "subclusters." The sums in definitions [2] and [4] of the gyration radius can be expanded:

$$\sum_{i=1}^{N}(\mathbf{r}_i - \mathbf{r}_0)^2 = \sum_{k=1}^{N_1}(\mathbf{r}_k - \mathbf{r}_0' + \mathbf{r}_0' - \mathbf{r}_0)^2 + \sum_{l=1}^{N_2}(\mathbf{r}_l - \mathbf{r}_0'' + \mathbf{r}_0'' - \mathbf{r}_0)^2. \qquad [A7]$$

Rearranging the terms of this equation with account for Eqs. [A1] and [A2] yields

$$\sum_{i=1}^{N}(\mathbf{r}_i - \mathbf{r}_0)^2 = \sum_{k=1}^{N_1}(\mathbf{r}_k - \mathbf{r}_0')^2 + \sum_{l=1}^{N_2}(\mathbf{r}_l - \mathbf{r}_0'')^2 + N_1(\mathbf{r}_0' - \mathbf{r}_0)^2 + N_2(\mathbf{r}_0'' - \mathbf{r}_0)^2. \qquad [A8]$$

Combining the two last terms of this equation with account for Eqs. [A4] and [A5] yields the following equation:

$$N^2R_g^2 = N\left(N_1R_1^2 + N_2R_2^2\right) + N_1N_2\Gamma^2, \qquad [A9]$$

where R_g, R_1, and R_2 are the gyration radii of the aggregate and its two parts, respectively. This equation is equivalent to Eq. [13].

In a specific case, when one of the subclusters consists of one sphere only (e.g., $N_2 = 1$), Eq. [A9] can be reduced to the following:

$$\Gamma^2 = \frac{N}{N-1}\left(NR_g^2 - R_2^2\right) - NR_1^2. \qquad [A10]$$

If the radii of gyration R_g and R_1 satisfy the scaling law [1] for N and $N-1$ spheres, respectively, Eq. [A10] yields Eq. [10], which is the basis of the SA algorithm. The second term on the right-hand sides of Eqs. [A10] and [10] must be omitted if the definition [2] is used instead of [4], which is equivalent to neglecting the gyration radius of a single spherule ($R_2 = 0$).

ACKNOWLEDGMENTS

The authors thank D. W. Mackowski and C. M. Sorensen for insightful discussions. The financial support of NASA Grant NAG3-1951, AFOSR Grant 97-1-0266, and NSF Grant CTS 990747 is gratefully acknowledged.

REFERENCES

1. Filippov, A. V., Markus, M. W., and Roth, P., *J. Aerosol Sci.* **30,** 71 (1999).
2. Hidy, G. M., and Brook, J. R., "The Dynamics of Aerocolloidal Systems." Pergamon, New York, 1970.
3. Mandelbrot, B. B., "The Fractal Geometry of Nature." W. H. Freeman, New York, 1983.
4. Mackowski, D. W., *Appl. Opt.* **34,** 3535 (1995).
5. Schmidt-Ott, A., Baltensperger, U., Gäggeler, H. W., and Jost, D. T., *J. Aerosol Sci.* **21,** 711 (1990).
6. Forrest, S. R., and Witten, T. A., *J. Phys. A: Math. Gen.* **12,** L109 (1979).
7. Meakin, P., *Rev. Geophys.* **29,** 317 (1991).
8. Köylü, Ü. Ö., Xing, Y., and Rosner, D. E., *Langmuir* **11,** 4848 (1995).
9. Neimark, A. V., Köylü, Ü. Ö., and Rosner, D. E., *J. Colloid Interface Sci.* **180,** 590 (1996).
10. Köylü, Ü. Ö., Faeth, G. M., Farias, T. L., and Carvalho, M. G., *Combust. Flame* **100,** 621 (1995).
11. Jullien, R., and Botet, R., "Aggregation and Fractal Aggregates." World Scientific, Singapore, 1987.
12. Sorensen, C. M., and Roberts, G. C., *J. Colloid Interface Sci.* **186,** 447 (1997).
13. Brasil, A. M., Farias, T. L., and Carvalho, M. G., *J. Aerosol Sci.* **30,** 1379 (1999).
14. Thouy, R., and Jullien, R., *J. Phys. A: Math. Gen.* **27,** 2953 (1994).
15. Cai, J., Lu, N., and Sorensen, C. M., *J. Colloid Interface Sci.* **171,** 470 (1995).
16. Köylü, Ü. Ö., and Faeth, G. M., *Combust. Flame* **89,** 140 (1992).
17. Hasmy, A., Foret, M., Pelous, J., and Jullien, R., *Phys. Rev. B* **48,** 9345 (1993).
18. Sorensen, C. M., *Aerosol Sci. Technol.*, in press.
19. Mountain, R. D., and Mulholland, G. W., *Langmuir* **4,** 1321 (1988).
20. Xing, Y., Köylü, Ü. Ö., and Rosner, D. E., *Appl. Opt.* **38,** 2686 (1999).
21. Oh, C., and Sorensen, C. M., *Phys. Rev. E* **57,** 784 (1998).
22. Chan, P., and Dahneke, B., *J. Appl. Phys.* **52,** 3106 (1981).
23. Morokoff, W. J., and Caflisch, R. E., *J. Comput. Phys.* **122,** 218 (1995).
24. Halton, J. H., *Numer. Math.* **2,** 84 (1960).
25. Filippov, A. V., and Rosner, D. E., *Int. J. Heat Mass Transfer* **43,** 127 (2000).
26. Bruning, J. H., and Lo, Y. T., *IEEE Trans. Antennas Propag.* **AP-19,** 378 (1970).
27. Jeffrey, D. J., and Onishi, Y., *J. Fluid Mech.* **139,** 261 (1984).
28. Mackowski, D. W., *J. Colloid Interface Sci.* **140,** 138 (1990).
29. Hobson, E. W., "The Theory of Spherical and Ellipsoidal Harmonics." Cambridge Univ. Press, New York, 1931.
30. Rogak, S. N., and Flagan, R. C., *J. Colloid Interface Sci.* **134,** 206 (1990).
31. Filippov, A. V., *J. Colloid Interface Sci.* **219,** 184 (2000).
32. Rosner, D. E., and Tandon, P., *AIChE J.* **40,** 1167 (1994).